This article has been accepted for publication in a future issue of this journal, but has not been fully edited. Content may change prior to final publication. Citation information: DOI 10.1109/ACCESS.2020.3028315, IEEE Access

Date of publication xxxx 00, 0000, date of current version xxxx 00, 0000.

Digital Object Identifier 10.1109/ACCESS.2017.DOI

A Dynamic Three-Bit Image Steganography Algorithm for Medical and e-Healthcare Systems

GHAZANFAR FAROOQ SIDDIQUI[1], ZAFAR IQBAL[1,2], KHALID SALEEM[1], (SENIOR MEMBER, IEEE), ZAFAR SAEED[1] , ADEEL AHMED[1], (MEMBER, IEEE) , IBRAHIM A. HAMEED[4], AND MUHAMMAD FAHAD KHAN [3]

[1]Department of Computer Science, Quaid-i-Azam University, Islamabad, Pakistan
[2]Department of Computer Science, Islamia University Bahawalpur, Punjab, Pakistan
[3]Department of Software Engineering, Foundation University Islamabad, Pakistan
[4]Department of ICT and Natural Sciences, Norwegian University of Science and Technology, 6009 Ålesund, Norway

Corresponding author: Zafar Iqbal (e-mail: mziqbal@cs.qau.edu.pk).

ABSTRACT Massive advances in internet infrastructure are impacting e-healthcare services compared to conventional means. Therefore, extra care and protection is needed for extremely confidential patient medical records. With this intention, we have proposed an enhanced image steganography method, to improve imperceptibility and data hiding capacity of stego images. The proposed Image Region Decomposition (IRD) method, embeds more secret information with better imperceptibility, in patient's medical images. The algorithm decomposes the grayscale magnetic resonance imaging (MRI) images into three unique regions: low-intensity, medium-intensity, and high-intensity. Each region is made up of k number of pixels, and in each pixel we operate the block of n least significant bits (LSBs), where $1 \leq n \leq 3$. Four classes of MRI images of different dimensions are used for embedding. Data with different volumes are used to test the images for imperceptibility and verified with quality factors. The proposed IRD algorithm is tested for performance, on the set of brain MRI images using peak signal-to-noise ratio (PSNR), mean square error (MSE) and structural similarity (SSIM) index. The results elucidated that the MRI stego image is imperceptible, like the original cover image by adjusting 2^{nd} and 1^{st} LSBs in the low-intensity region. Our proposed steganography technique provides a better average PSNR (49.27), than other similar methods. The empirical results show that the proposed IRD algorithm, significantly improves the imperceptibility and data embedding capacity, compared to the existing state-of-the-art methods.

INDEX TERMS Data Payload, Image Region Decomposition, LSB, MRI, Spatial Domain, Steganography.

I. INTRODUCTION

Over the years, the infrastructure of the Internet has expanded significantly from urban to rural areas. Nowadays, images are the main component of multimedia content [1], [2]. With the massive and rapid development of the Internet and network infrastructure, is a common way of using image steganography methods to hide confidential data in different image modalities [3]. A large number of changes in the computing world, including hardware, software, and networks, have created threats to copyright protection and content integrity. Steganography systems are used for invisible communication to embed secret data bits in any communication medium [4]. Information concealment techniques are used to exchange confidential data, withstanding intruders attacks (passive or active). Passive steganalysis exposes the absence / presence of secret data in the stego medium. In contrast, active steganalysis focuses on finding important attributes like original confidential data, data length, location, secret key, and so on [5]. The primitive types of steganography schemes are: spatial domain and transform or frequency domain [6]. In spatial domain schemes, the bits of the pixel values are directly exploited. The most popular spatial domain steganography schemes are based on the least significant bit substitutions [7]–[15]. In the frequency domain, transformation-based schemes are implemented [4], [16]–[20]. Over the years, the steganography of images has been studied significantly and categorized as reversible and irreversible. The recovery of the hidden data and the restoration of the original image is a focal point of the reversible techniques. At the same time, the irreversible methods mainly focus on the recovery of the hidden data [21]. The telemedicine framework allows healthcare facilities to be available in geographically isolated areas to monitor a patient's condition remotely [22]. A patient's medical reports are highly confidential and require special attention when sharing over networks. In e-healthcare systems, the protection of sensitive data requires special attention from a security perspective [23]. Usually, description of images is provided as text. If there is no text report accompanying the image, based on the opinion of the radiologist, the image appears incomprehensible unless some specialists see it [24]. Images can be altered with false information and redistributed to defame a person or organization. Therefore a significant need for content protection. Steganography has become a sufficient solution for such scenarios [25]. In a simple steganography technique, images are more likely to steal confidential information [26]. We have developed an efficient IRD image steganography scheme with better built-in secret data protection. In our steganography technique, sensitive patient diagnostic reports and other secret information are integrated into MRI images with good imperceptibility and high payload capacity. Our embedding procedure (Algorithm 1) embeds data up to 3^{rd} LSB of host images without any clue for the third party on secret information. The embedding procedure is used at the sender side, to hide confidential patient reports, and the reverse procedure is used for extracting secret data from the receiver side. Our goal is to hide a patient's medical information in MRI images with improved imperceptibility and data payload capacity so that the patient's medical history is easily accessible to the consultant from MRI images. Mathematically, steganography is defined as:

$$Stego = Embed(c, m, k). \tag{1}$$

$$Message = Ext(s). \tag{2}$$

Here, $Embed$ and Ext are the mapping functions for embedding and extracting data in (1) and (2), respectively. Where c is the cover medium, the secret key is denoted by k, and the stego medium is denoted by s with secret data message m. **Our key contributions are as follow**:

- Optimization of the threshold value t_1 and t_2 for image segmentation into three unique regions.
- Performed various mathematical operations to exploit the bits of each pixel up to 3^{rd} LSB for data embedding.
- Minimization of pixel value difference for t_1 with the adjustment of 1^{st} and 2^{nd} LSB while the minimization of difference for t_2 with the adjustment of 1^{st} LSB.
- Introduced a novel method with significant performance in the context of imperceptibility and payload capacity.
- Carrying out a detailed evaluation and comparison of performance with other similar state-of-the-art procedures.

II. RELATED WORK

Liao et al. [27] used the interblock technique for embedding purposes. JPEG (Joint Photographic Experts Group) images are considered a host or stego image. This technique is specific to medical JPEG images to hide patient records. Adjacent discrete cosine transform (DCT) blocks of similar positions are used to calculate the difference between the coefficients. The work of Sajjad et al. [28] is based on the detection of the region of interest (ROI) and then embedding this ROI to the host image. Some cloud resources are used for encryption of stego images and then transmitted to the receiver over any medium. The receiving side performs the decryption procedure to separate the ROI from the host image and can be used by the concerned consultant. Alsaidi et al. [29] Analyzes the use of steganography in computer forensics and explains how criminals can use it to hide evidence. In addition, their research offers study directions for forensic experts. According to Elhoseny et al. [30], nowadays Internet of Things (IoT) devices play an important role in healthcare systems. Level 1 and 2 2D discrete wavelet transform techniques are used to embed patient data in any cover medium. Grayscale and color images are used for cover images. Standard encryption is applied to text data before embedding into the cover media. Various statistical measures are applied to verify the imperceptibility of the cover medium. Statistical scoring works best for secret textual information compared to similar existing techniques [31]. Biometric systems face many security and data integrity challenges. Steganography can play an important role in biometric security. LSB and PVD based steganography methods are widely used to protect biometric data and resist various statistical attacks. Shehab et al. [32] present a delicate watermark technique for self-retrieval and authentication of images in medical applications. A singular value decomposition (SVD) scheme is used on the blocks of the broken image. The SVD block-wise tracks are substituted to the host image LSBs. The technique worked well to recover the original data in case of tampering with the host image. Lee [33] uses the reversible watermark technique on the segmented image, the background region and the object region. If tampering or forgery has been done to image modalities such as X-rays, computed tomography (CT) or MRI images, the proposed techniques work well to detect the tampering using the hash code. The reversible watermark techniques are particularly effective where medical systems are more vulnerable to forgery or tampering. Kaw et al. [34] offer a method of incorporating data based on optical pixel repetition to integrate patient records into their clinical images. The proposed technique divides the cover image into two by two blocks. Each block contains 16 possible arrangements with four pixel positions. The electronic patient record is integrated into each block by substituting secret data bits to each block pixel bits. The work of Parah et al. [35] is based on dividing the host image into non-overlapping blocks of n^{th} size. These blocks are based on both non-seed pixels and seed pixels. Only non-seed pixels are used for data embedding to achieve better imperceptibly and payload capacity. The selection of image pixels from the non-sequential least significant bits is based on pixel similarity and fuzzy logic. Pixels with similar intensity values are used to embed secret patient data. The patient's electroencephalogram (EEG) signal data is used for integration into the MRI host images of the patient [36]. With the increase in popularity of the Internet, people want to share images, videos, documents on the transmission medium. There has been a need to prevent the data from being lost using digital steganography. In addition, information security has a high demand due to the growing concern of the digital market [15]. The imperceptibility and the payload capacity are somehow inversely proportional to each other. If one factor decreases, the other will be increased [37]. The persistence capability is high when the stego media is secured for data elimination and warp attacks. Robustness is the main concern of watermarking algorithms while imperceptibility and storage capacity are major concerns of steganography [2]. The Authors Sahu and Swain have implemented very useful data embedding techniques to improve PSNR and data embedding capability; double layer reversible data embedding method to embed the data in four images [21]. Reversible data embedding method for embedding data in pixels of similar images using LSB match [6]. The right-most n-bit replacement technique uses a pair of similar pixels [3]. The technique of pixel value differencing and modulus function with minimization of the fall of the boundary problem [38]. The rightmost n bits are used for embedding where n is between one and four [39]. The pixel overlap block is based on five pixels from the right, this block is divided into four sub-blocks, 1^{st} and 5^{th}, 2^{nd} and 5^{th}, 3^{rd} and 5^{th}, 4^{th} and 5^{th} [40]. The bit flipping method works on 7^{th} and 8^{th} to hide secret data in cover images [41]. The work of Wazirali and Chachzo [42] divides the regions of the image into non-edge and edge regions. The secret data can only be integrated into the image of the edge region. Zero crossings and log mask with grouping are used to divide the image into edge and not edge regions. Wang and Qian [43] in 2018 came up with improvements to the existing distortion feature for jpeg images. The minimization of image distortion is caused by the embedding procedure. A reference image was built before compression which is close to the original host image. Li et al. [44] introduced a technique for embedding data into multiple images known as batch steganography, unlike traditional steganography where only one image is used at a time for embedding purposes. Secret data bits can be retrieved from more than one share, in case of unusual condition in the communication medium during data transmission [44]. Communication channels are widely suitable for compressed jpeg images. Before sending it to the channel, an intermediate image is created, which is close enough to stego image. Tao applied the coefficient adjustment compression scheme in this way so that the original stego image and the compressed image remain similar [45]. Li and Zhang [46] proposed a significant technique for hiding secret data in a fingerprint image, constructed directly from a hidden message. There is no need for a cover signal for embedding purposes, like conventional steganography schemes. The secret message is used as a piece of the hologram to construct the fingerprint image and mapped to the polynomial and encoded at different points of polarities [46].

III. PROPOSED METHOD

Our proposed algorithm dynamically segments the image into three regions based on intensity and exploits pixel bytes up to 3^{rd} LSB. The three unique regions are low intensity, medium intensity, and high intensity, denoted by L, M, and H respectively. The threshold value t_1 and t_2 divides the image into three unique regions. The size of each region can vary dynamically from image to image. In the low intensity (first) region, we exploit pixel bits up to three least significant bits. Secret patient data integrated into third LSB with adjustment of 1^{st} and 2^{nd} LSB, while medium intensity region (second) works with 2^{nd} LSB with the adjustment of 1^{st} LSB. In the high intensity (third) region, only 1^{st} LSB is used for data embedding. These three gray level ranges are used for the incorporation of secret data. Our proposed embedding Algorithm 1 first reads random grayscale values using the pixel index, if the value is in the first region, modify the 3^{rd} LSB and maintain image quality with improvement of 2^{nd} and 1^{st} LSB. In the case of the second region, only 2^{nd} LSB is used with the adjustment of 1^{st} LSB and if the pixel intensity value is in the region 3^{rd}, only the first LSB is operated. A secret key is calculated to randomly select the pixel index value before the embedding and extracting procedures. The real number range of 2 to 9 is used to calculate the value of the secret key. If someone intercepts the stego image media LSBs, they will not be able to completely destroy the secret data. At the most, they could attempt to change all (three) LSBs, which will drastically decrease the visual quality and make the stego image noticeable to human eyes. The Figure 1 illustrates the proposed IRD methodology.

A. EMBEDDING PROCEDURE

The embedding Algorithm 1 first calculates the bytes available in the host image for modification. If the host image capacity bytes available for embedding is less than or equal to the size of SDB, the embedding process will start otherwise an error has occurred. The secret data bits are integrated one by one with the LSBs in the host image. If the pixel intensity range is in the first region, modify 3^{rd} LSB and adjust the 2^{nd} and 1^{st} LSB. If the pixel intensity range is in the second region, then modify 2^{nd} LSB and adjust the 1^{st} LSB, and if the pixel intensity range is in the third region, modify 1^{st} LSB only.

If the gray level range is 0 to 85 then change the third bit with the adjustment of 2^{nd} and a 1^{st} bit.

$$0\,0\,1\,0\,1\,0\,1\,0 \longrightarrow 0\,0\,1\,0\,1\,\underline{\mathbf{0\,1\,0}}$$

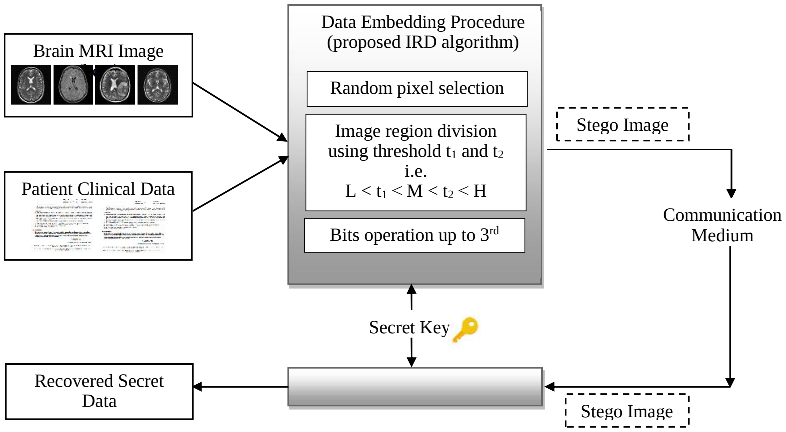

FIGURE 1. Block diagram of the IRD steganographic system.

If the gray level range is 86 to 170 then change the second bit with the adjustment of the 1^{st} bit.

$$1\,0\,0\,0\,0\,0\,1\,0 \longrightarrow 1\,0\,0\,0\,0\,0\,\underline{\mathbf{1}\,\mathbf{0}}$$

If the gray level range is 171 to 255 then change the 1^{st} LSB.

$$1\,1\,1\,1\,0\,0\,1\,0 \longrightarrow 1\,0\,0\,0\,0\,0\,1\,\underline{\mathbf{0}}$$

B. EXTRACTION PROCEDURE

The extraction process will begin by reading the grayscale pixel index values from the stego image using the secret key. The Algorithm 2 describes the extraction procedure in detail.

C. EXAMPLE OF PROPOSED IRD ALGORITHM

1) Embedding Example

Step 1: Suppose, the randomly selected pixel value of the host image in decimal is 84 (gVal), equal to $(01010100)_2$ and the embedding bit stream is 01010100. We used threshold t_1=86 and t_2=171. The selected pixel value (84) belongs to low-intensity (L) region because the selected value is less than threshold t_1.

Step 2: As L intensity region is considered among the three low (L), medium (M), and High (H). now the logical AND operation performed with constant value 7, equal to $(111)_2$. $(01010100)_2 \wedge (111)_2 = (00000100)_2$ (Hold) and the first bit of embedding bit stream is 0 (SDB=zero).

Step 3: As per Algorithm 1 $(01010100)_2$ subtraction $(100)_2$ = $(01010000)_2$ perform subtraction with 4. $(01010000)_2$ Addition $(011)_2 = (01010011)_2$ perform addition with 3. After SDB substitution the new pixel value (gVal) is $(01010011)_2$ = 83 in decimal.

Step 4: Suppose, the randomly selected pixel value of host image in decimal is 154 (gVal), equal to $(10011010)_2$ for the same embedding bit stream. The selected pixel value (154) belongs to Medium-intensity (M) region because the selected value lies between threshold t_1 and t_2. Now the logical AND operation performed with constant value 3, equal to $(011)_2$. $(10011010)_2 \wedge (011)_2 = (00000010)_2$ (Hold) and the first bit of embedding bit stream is 0 (SDB=zero).

Step 5: As per Algorithm 1 $(10011010)_2$ subtraction $(010)_2$ = $(10011000)_2$. perform subtraction with 2. $(10011000)_2$ Addition $(001)_2$ = $(10011001)_2$. perform addition with 1. After SDB substitution the new pixel value (gVal) is $(10011001)_2$ = 153 in decimal.

Step 6. Suppose, the randomly selected pixel value of host image in decimal is 237 (gVal), equal to $(11101101)_2$ for the same embedding bit stream. The selected pixel value (237) belongs to High-intensity (H) region because the selected value is greater than threshold t_2. As per Algorithm 1 $(11101101)_2 \wedge (11111110)_2 = (11101100)_2$, next $(11101100)_2 \vee$ (SDB) = $(11101100)_2$. After SDB substitution the new pixel value (gVal) is $(11101100)_2$ = 236 in decimal.

Step 7: Embedding is done for three cases. The embedding bits are $(000)_2$.

2) Extraction Example

Step 1: Suppose the randomly selected pixel value is $(01010011)_2$ = 83 (gVal is less than threshold t_1). The bit value of third LSB is extracted, which is 0 now.

Step 2: Suppose the pixel value is $(10011001)_2$ = 153 in decimal (gVal lies between threshold t_1 and t_2). The bit value of second LSB is extracted, which is 0 now.

Step 3: Suppose the pixel value is $(11101100)_2$ = 236 in decimal (gVal is greater than threshold t_2). The bit value of first LSB is extracted, which is 0 now.

Step 4: The extracted bits are $(000)_2$. Extraction is done.

D. ERROR METRICS

Two common error metrics, MSE, PSNR [47] and an SSIM quality metric are used to compare the image degradation between the original and stego images. Suppose we have two $m \times n$ image dimension, x and y, then MSE, PSNR and SSIM are displayed in (3), (4) and (5), where MAXI is 255 for gray images.

Algorithm 1: Secrete Data Embedding

```
Input  : Cover / host Image, Secret data bits (SDB)
Output: Stego Image
Compute secret data bits size
Check host image pixel intensity value, for example
  its $gVal$
repeat
    Acquire next $gVal$ and $SDB$
    if $gVal \in$ FIRST region then
        $HOLD \leftarrow gVal \wedge 7$
        if $HOLD \leq 3$ and $SDB = 0$ then
            $gVal \leftarrow gVal \vee HOLD$
        else if $HOLD \leq 3$ and $SDB = 1$ then
            $gVal \leftarrow gVal \vee 7$
            $gVal \leftarrow gVal - 3$
        else if $HOLD > 3$ and $SDB = 1$ then
            $gVal \leftarrow gVal \vee HOLD$
        else if $HOLD > 3$ and $SDB = 0$ then
            $gVal \leftarrow gVal - 4$
            $gVal \leftarrow gVal + 3$
        else
            Continue
    else if $gVal \in$ SECOND region then
        $HOLD \leftarrow gVal \wedge 3$
        if $HOLD \leq 1$ and $SDB = 0$ then
            $gVal \leftarrow gVal \vee HOLD$
        else if $HOLD \leq 1$ and $SDB = 1$ then
            $gVal \leftarrow gVal \vee 3$
            $gVal \leftarrow gVal - 1$
        else if $HOLD > 1$ and $SDB = 1$ then
            $gVal \leftarrow gVal \vee HOLD$
        else if $HOLD > 1$ and $SDB = 0$ then
            $gVal \leftarrow gVal - 2$
            $gVal \leftarrow gVal + 1$
        else
            Continue
    else
        $gVal \leftarrow gVal \wedge 254$
        $gVal \leftarrow gVal \vee SDB$
until the embedding of last $SDB$
```

Algorithm 2: Data Extraction Procedure

```
Input  : Stego Image
Output: Secrete Data
repeat
    if $gVal \in$ Low-intensity region then
        Read the bit value of third LSB    ▷ i.e., $t_1$
    else if $gVal \in$ Medium-intensity region then
        Read the bit value of second LSB  ▷ i.e., $t_2$
    else
        Read the bit value of first LSB
until all secret data bits are extracted
```

$$MSE = \frac{1}{n \times m} \sum_{i=0}^{m-1} \sum_{j=0}^{n-1} [x(i,j) - y(i,j)]. \tag{3}$$

$$PSNR = 10 \times \log_{10} \left(\frac{MAXI^2}{MSE} \right). \tag{4}$$

$$SSIM(x,y) = [l(x,y)] \cdot [c(x,y)] \cdot [s(x,y)]. \tag{5}$$

The SSIM function is based on the following three components: the luminance similarity in (6), the contrast similarity in (7), and the structural similarity (8). These are calculated as follows for the two images x and y [47].

$$l(x,y) = \left(\frac{2\mu x \, \mu y + c1}{\mu_x^2 + \mu_y^2 + c1} \right). \tag{6}$$

$$c(x,y) = \left(\frac{2\sigma_x \sigma_y + c2}{\sigma_x^2 + \sigma_y^2 + c2} \right). \tag{7}$$

$$s(x,y) = \left(\frac{\sigma_{xy} + c3}{\sigma_x \sigma_y + c3} \right). \tag{8}$$

The mean values of the original and processed image are denoted by μx, μy, and the standard deviation of the original and processed image is defined by σ_x and σ_y. The co-variance of x and y images is denoted by σ_{xy}. c1, c2, and c3 represent constant values [47].

IV. EXPERIMENTAL SETUP

We have used sample images from a well know data repository[1] to test our method on various images with a variety of dimensions as given in Table 1.

TABLE 1. Set of MRI images of variable dimensions with variable embedding data size.

Image Dimension	No of images	Variable size data for embedding
128 × 128	20	1KB, 2KB
256 × 256	20	2KB, 4KB, 8KB
512 × 512	20	8KB, 16KB, 32KB
1024 × 1024	20	50KB, 100KB, 130KB
1024 × 1024	20	62KB (patient report size)

We considered twenty cases for each set of variable dimension for our experiments. The images in Figure 2 from $n1$ to $n10$ are negative or normal images without cancer, and the images from $p1$ to $p10$ are positive or abnormal cases with cancer. The purpose of using variable size embedding data is to test the performance and the real strength of the proposed algorithm.

We tested our proposed algorithm with four image dimensions with ten different payload configurations, as shown in Table 1. We used MSE, PSNR, and SSIM as evaluation matrices for images of various dimensions and the embedding data of different sizes for the performance.

[1] (https://www.kaggle.com/navoneel/brain-mri-images-for-brain-tumor-detection) (accessed on February 24, 2020)

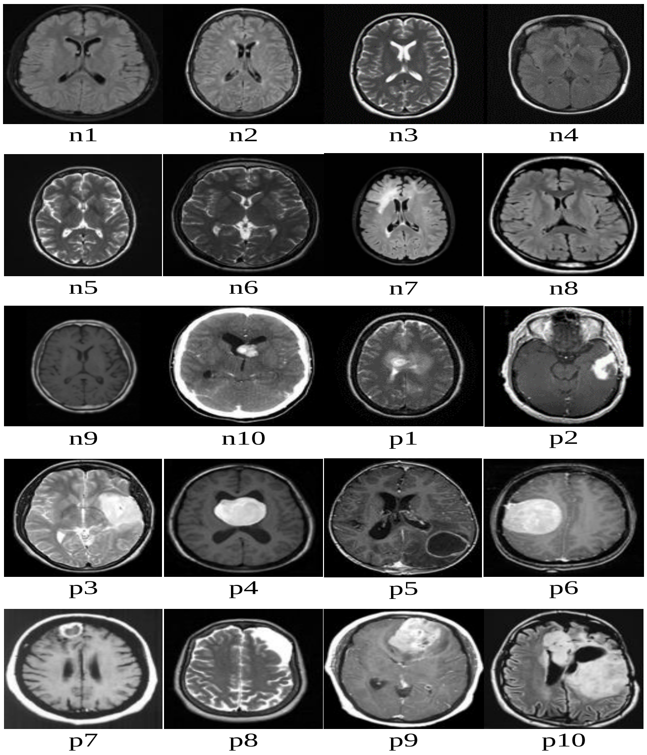

FIGURE 2. The set of MRI grayscale BMP host images for experiments. n1 to n10 are negative cases and p1 to p10 are positive cases.

V. RESULTS AND ANALYSIS

We compare our algorithm at 100% payload capacity of host images. Analysis of MSE, PSNR, and SSIM shows that the stego images are highly imperceptible and cannot be discriminated by human eyes. The average PSNR 45.61 and SSIM 0.974 respectively for 1KB payload, while for 2KB payload it is 41.29 and 0.953 as shown in Table 2.

TABLE 2. Results of stego images of 128×128 dimension, having 1KB and 2KB embedding data size.

	1KB			2KB		
No	MSE	PSNR	SSIM	MSE	PSNR	SSIM
n1	1.88	45.38	0.991	4.92	41.20	0.990
n2	1.64	45.96	0.977	4.72	41.39	0.955
n3	1.31	46.93	0.995	4.02	42.08	0.994
n4	1.63	45.98	0.99	4.72	41.38	0.985
n5	1.47	46.43	0.992	4.35	41.73	0.990
n6	1.62	46.00	0.987	4.73	41.37	0.987
n7	1.92	45.28	0.965	5.31	40.87	0.916
n8	2.20	44.69	0.957	5.75	40.52	0.912
n9	2.09	44.91	0.947	5.84	40.46	0.883
n10	2.10	44.90	0.951	5.31	40.87	0.916
p1	2.18	44.73	0.956	5.55	40.68	0.920
p2	2.23	44.64	0.953	5.59	40.65	0.913
p3	2.04	45.01	0.954	5.11	41.04	0.921
p4	1.93	45.26	0.970	5.19	40.97	0.950
p5	2.23	44.63	0.962	5.68	40.58	0.933
p6	1.47	46.43	0.990	4.27	41.81	0.989
p7	1.43	46.55	0.992	3.67	42.48	0.992
p8	1.35	46.79	0.987	4.07	42.02	0.983
p9	1.95	45.22	0.959	4.87	41.25	0.938
p10	1.47	46.44	0.995	3.77	42.36	0.995
Avg	1.81	45.61	0.974	4.87	41.29	0.953

Secret data of various sizes, up to 100% capacity of MRI host images are embedded to test imperceptibility and payload capacity. Images of dimension 256 × 256 are tested on three different payloads i.e., 2KB, 4KB, and 8KB. Table 3 shows the results on MSE, PSNR, and SSIM. The average PSNR value for 2KB, 4KB and 8KB is 45.09 and SSIM is 0.966.

TABLE 3. Results of stego images of 256×256 dimension, having 2KB, 4KB, and 8KB embedding data size.

	2KB			4KB			8KB		
No	MSE	PSNR	SSIM	MSE	PSNR	SSIM	MSE	PSNR	SSIM
n1	1.29	47.01	0.987	2.31	44.47	0.983	3.09	43.22	0.987
n2	1.22	47.25	0.986	2.06	44.99	0.954	2.63	43.92	0.942
n3	1.06	47.85	0.988	1.73	45.73	0.991	2.17	44.75	0.991
n4	1.28	47.03	0.985	2.09	44.92	0.985	2.97	43.39	0.984
n5	1.15	47.51	0.988	1.82	45.52	0.989	2.60	43.97	0.988
n6	1.23	47.21	0.988	2.05	44.99	0.984	2.73	43.75	0.983
n7	1.39	46.69	0.986	2.44	44.25	0.927	3.41	42.80	0.894
n8	1.51	46.33	0.982	2.63	43.91	0.951	3.79	42.34	0.909
n9	1.54	46.25	0.973	2.68	43.84	0.931	3.91	42.20	0.880
n10	1.38	46.71	0.983	2.51	44.12	0.946	3.29	42.95	0.918
p1	1.45	46.51	0.981	2.58	44.00	0.948	3.63	42.53	0.916
p2	1.43	46.55	0.983	2.69	43.82	0.944	3.58	42.58	0.914
p3	1.33	46.88	0.985	2.41	44.30	0.948	3.07	43.24	0.921
p4	1.38	46.71	0.983	2.37	44.38	0.962	3.23	43.02	0.941
p5	1.47	46.43	0.983	2.61	43.95	0.959	3.70	42.44	0.930
p6	1.13	47.58	0.990	1.83	45.50	0.984	2.23	44.63	0.985
p7	0.98	48.18	0.989	1.69	45.85	0.99	2.25	44.59	0.989
p8	1.05	47.88	0.990	1.71	45.79	0.978	1.99	45.13	0.975
p9	1.29	47.01	0.986	2.30	44.49	0.956	2.84	43.58	0.936
p10	1.01	48.07	0.993	1.82	45.52	0.994	2.17	44.76	0.995
Avg	1.27	47.08	0.985	2.21	44.71	0.965	2.96	43.48	0.948

We evaluate the IRD method on a higher dimension, 512 × 512, and embedding data up to 32KB. The results for 8KB, 16KB and 32KB are shown in Table 4. The average PSNR for the given payload is 46.21, and the SSIM is 0.963, respectively.

TABLE 4. Results of stego images of 512×512 dimension, having 8KB, 16KB, and 32KB embedding data size.

	8KB			16KB			32KB		
No	MSE	PSNR	SSIM	MSE	PSNR	SSIM	MSE	PSNR	SSIM
n1	0.82	48.94	0.988	1.76	45.66	0.982	3.17	43.11	0.982
n2	0.67	49.81	0.962	1.50	46.35	0.966	2.78	43.67	0.934
n3	0.54	50.74	0.995	1.21	47.29	0.994	2.29	44.52	0.990
n4	0.73	49.46	0.99	1.49	46.37	0.983	2.93	43.44	0.985
n5	0.63	50.13	0.991	1.28	47.02	0.985	2.56	44.04	0.989
n6	0.67	49.85	0.985	1.49	46.39	0.984	2.81	43.63	0.980
n7	0.87	48.69	0.955	1.92	45.28	0.958	3.65	42.50	0.873
n8	1.00	48.09	0.98	2.09	44.92	0.954	3.96	42.14	0.893
n9	1.04	47.92	0.964	2.16	44.77	0.934	4.16	41.93	0.858
n10	0.89	48.62	0.979	1.96	45.19	0.948	3.46	42.73	0.903
p1	0.93	48.40	0.978	2.06	44.97	0.950	3.78	42.34	0.900
p2	0.95	48.34	0.977	2.17	44.74	0.946	3.77	42.35	0.898
p3	0.84	48.88	0.979	1.86	45.39	0.950	3.25	43.00	0.906
p4	0.85	48.81	0.973	1.81	45.55	0.966	3.37	42.84	0.933
p5	0.97	48.23	0.979	2.04	45.02	0.961	3.84	42.28	0.919
p6	0.56	50.64	0.986	1.26	47.09	0.986	2.30	44.51	0.982
p7	0.60	50.32	0.990	1.23	47.20	0.988	2.19	44.71	0.986
p8	0.5	51.06	0.980	1.13	47.58	0.982	2.08	44.94	0.971
p9	0.78	49.15	0.982	1.76	45.65	0.958	2.96	43.41	0.926
p10	0.58	50.49	0.995	1.37	46.75	0.994	2.23	44.62	0.995
Avg	0.77	49.33	0.980	1.68	45.96	0.968	3.08	43.34	0.940

The payload size increases to 130KB for 1024×1024 dimension images. The average PSNR for 50KB, 100KB and 130KB is 45.03 and SSIM 0.974, shown in the Table 5.

TABLE 5. Results of stego images of 1024×1024 dimension, having 50KB, 100KB, and 130KB embedding data size.

	50KB			100KB			130KB		
No	MSE	PSNR	SSIM	MSE	PSNR	SSIM	MSE	PSNR	SSIM
n1	1.40	46.66	0.990	2.40	44.32	0.985	3.160	43.12	0.987
n2	1.13	47.57	0.986	2.07	44.95	0.959	2.750	43.72	0.986
n3	0.87	48.73	0.996	1.73	45.72	0.992	2.230	44.62	0.996
n4	1.10	47.70	0.989	2.40	44.62	0.986	3.000	43.35	0.987
n5	0.93	48.41	0.990	1.99	45.13	0.989	2.590	43.98	0.988
n6	1.04	47.93	0.990	2.28	44.54	0.984	2.800	43.64	0.986
n7	1.47	46.43	0.985	2.62	43.94	0.949	3.540	42.63	0.968
n8	1.67	45.89	0.967	2.79	43.66	0.953	3.910	42.20	0.960
n9	1.59	46.10	0.959	3.21	43.05	0.915	4.060	42.04	0.947
n10	1.56	46.19	0.961	2.55	44.06	0.949	3.400	42.80	0.963
p1	1.60	46.07	0.965	2.82	43.62	0.945	3.740	42.39	0.953
p2	1.67	45.88	0.963	2.91	43.48	0.939	3.700	42.44	0.962
p3	1.51	46.33	0.964	2.30	44.49	0.951	3.210	43.06	0.966
p4	1.39	46.67	0.976	2.47	44.19	0.964	3.370	42.85	0.974
p5	1.60	46.08	0.969	2.79	43.66	0.963	3.820	42.30	0.968
p6	0.92	48.46	0.992	1.67	45.90	0.985	2.270	44.55	0.988
p7	0.99	48.15	0.991	1.60	46.08	0.992	2.210	44.67	0.990
p8	0.84	48.85	0.991	1.57	46.14	0.979	2.070	44.96	0.991
p9	1.36	46.76	0.968	2.20	44.69	0.962	2.950	43.43	0.971
p10	1.08	47.79	0.995	1.75	45.69	0.996	2.200	44.69	0.995
Avg	1.29	47.13	0.979	2.31	44.60	0.967	3.05	43.37	0.976

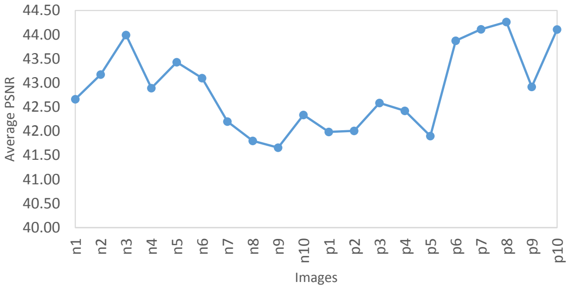

FIGURE 3. Average PSNR for image dimensions 128×128, 256×256, 512×512, 1024×1024 at maximum payload.

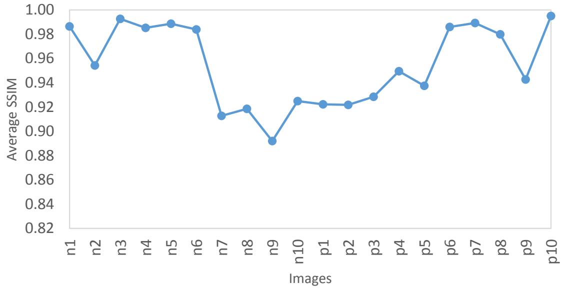

FIGURE 4. Average SSIM for image dimensions 128×128, 256×256, 512×512, 1024×1024 at maximum payload.

Figures 3 and 4 respectively visualize the average PSNR and SSIM at maximum payload for four dimensions 128×128, 256×256, 512×512, 1024×1024. Each dimension contains twenty images. The maximum average PSNR and SSIM at maximum payload for all four dimension images is 43.40 and 0.955 respectively.

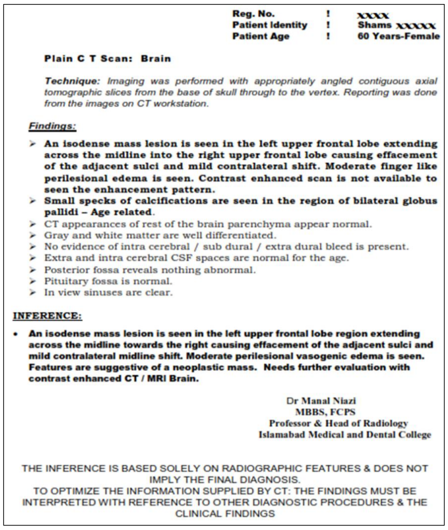

Reg. No. ! XXXX
Patient Identity ! **Shams XXXXX**
Patient Age ! **60 Years-Female**

Plain C T Scan: Brain

Technique: *Imaging was performed with appropriately angled contiguous axial tomographic slices from the base of skull through to the vertex. Reporting was done from the images on CT workstation.*

Findings:

- **An isodense mass lesion is seen in the left upper frontal lobe extending across the midline into the right upper frontal lobe causing effacement of the adjacent sulci and mild contralateral shift. Moderate finger like perilesional edema is seen. Contrast enhanced scan is not available to seen the enhancement pattern.**
- **Small specks of calcifications are seen in the region of bilateral globus pallidi – Age related**.
- CT appearances of rest of the brain parenchyma appear normal.
- Gray and white matter are well differentiated.
- No evidence of intra cerebral / sub dural / extra dural bleed is present.
- Extra and intra cerebral CSF spaces are normal for the age.
- Posterior fossa reveals nothing abnormal.
- Pituitary fossa is normal.
- In view sinuses are clear.

INFERENCE:

- **An isodense mass lesion is seen in the left upper frontal lobe region extending across the midline towards the right causing effacement of the adjacent sulci and mild contralateral midline shift. Moderate perilesional vasogenic edema is seen. Features are suggestive of a neoplastic mass. Needs further evaluation with contrast enhanced CT / MRI Brain.**

Dr Manal Niazi
MBBS, FCPS
Professor & Head of Radiology
Islamabad Medical and Dental College

THE INFERENCE IS BASED SOLELY ON RADIOGRAPHIC FEATURES & DOES NOT IMPLY THE FINAL DIAGNOSIS.
TO OPTIMIZE THE INFORMATION SUPPLIED BY CT: THE FINDINGS MUST BE INTERPRETED WITH REFERENCE TO OTHER DIAGNOSTIC PROCEDURES & THE CLINICAL FINDINGS

FIGURE 5. Patient sample report.

Furthermore, the proposed method is tested on real patient's data[2] as shown in Figure 5. The results elucidated that the stego images are visually imperceptible to human eyes and almost similar to the original host images, as shown in Figure 6 and maintain a better PSNR value as shown in the Table 6.

The Table 6 presents the result of the stego images embedded with patient report. the average PSNR value is 45.94, and the average SSIM is 0.98, respectively.

TABLE 6. Results of stego images of 1024×1024 dimension, having 62KB patient report.

	62KB (patient report)		
No	MSE	PSNR	SSIM
n1	1.63	45.99	0.982
n2	1.36	46.79	0.980
n3	1.06	47.85	0.997
n4	1.30	46.96	0.993
n5	1.10	47.69	0.994
n6	1.30	46.97	0.987
n7	1.77	45.62	0.968
n8	1.96	45.20	0.982
n9	1.99	45.13	0.972
n10	1.83	45.48	0.978
p1	1.92	45.28	0.972
p2	2.03	45.04	0.976
p3	1.75	45.68	0.979
p4	1.66	45.90	0.982
p5	1.90	45.32	0.983
p6	1.10	47.69	0.988
p7	1.12	47.62	0.991
p8	0.99	48.13	0.989
p9	1.63	46.00	0.982
p10	1.24	47.19	0.997
Avg	1.53	46.38	0.984

[2] *Courtesy: Akbar Niazi Teaching Hospital Islamabad* https://www.anth.pk (accessed on October 15, 2019)

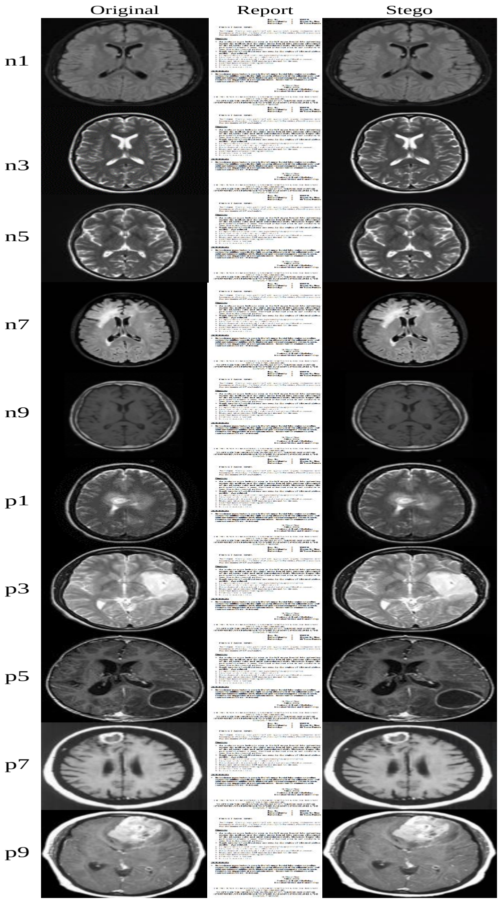

FIGURE 6. Visual results of embedding patient's sample report to set of MRI host images, having dimension 1024×1024.

Figures 7 and 8 show the visual trend of PSNR and SSIM values, respectively. The maximum PSNR and SSIM values are calculated for stego image $N3$. The average PSNR value is over 45db and SSIM is very close to 1.

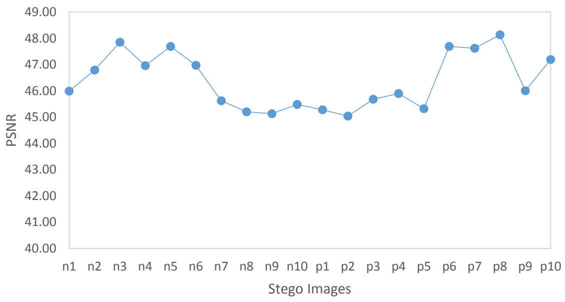

FIGURE 7. Visual comparison of stego images PSNR for patient report.

The proposed method maintains the visual degradation of stego images to make them imperceptible and better payload capacity in terms of MSE, PSNR, SSIM, and bpp.

Loan et al. [48] performed experiments on the set of randomly selected medical images as shown in Figure 9, as well as on commonly available standard image processing images. we performed our experiments on a similar set of images for comparison purpose. The set of medical images consist of a standard size 512×512.

VI. EVALUATION AND DISCUSSION

The performance comparison of the proposed IRD method with the state-of-the-art technique [48] on the set of randomly selected medical images from UCID dataset[3] is shown in Table 7. The comparison of results with standard set of images that are commonly used in image processing are presented in Table 10 and Table 9. The average PSNR, SSIM, and bpp by [48] is 41.60, 0.982, and 0.816 respectively. Our proposed technique obtained better average PSNR and bpp, which are 43.20 and 1.03 respectively.

TABLE 7. Performance comparison of PSNR and SSIM on the set of randomly chosen medical images with the state-of-the-art technique.

	Loan et al. [48]		Proposed method	
Sr. No	PSNR	SSIM	PSNR	SSIM
Image 1	43.86	0.986	46.61	0.993
Image 2	48.24	0.991	45.54	0.987
Image 3	45.14	0.990	44.76	0.989
Image 4	44.62	0.990	44.70	0.993
Image 5	46.97	0.990	43.61	0.978
Image 6	43.58	0.981	41.33	0.844
Image 7	44.35	0.981	41.08	0.822
Image 8	37.66	0.984	43.35	0.986
Image 9	28.03	0.959	41.02	0.797
Image 10	33.50	0.968	40.29	0.757
Avg	41.60	0.982	43.23	0.915

Table 8 shows the PSNR results at different threshold values. The threshold value t_1 and t_2 have a direct impact on the size of the image region. Threshold t_1 is significant, because as its value increases, the PSNR decreases because t_1 resizes the first region based on low intensity, which exploits the pixel value up to 3^{rd} LSB. The results of our experiment are based on t_1, t_2 with values of 86 and 171 respectively, as this divides the intensity ranges into three balanced portion.

Figure 10 shows the impact of the threshold t_1 on the average PSNR values for a standard set of images. Table 8 reveals the detail of various t_1 and t_2 values with their respective region sizes while Figure 10 is based only on the considered t_1 value.

[3](http://homepages.lboro.ac.uk/cogs/datasets/ucid/data/ucid.v2.tar.gz)

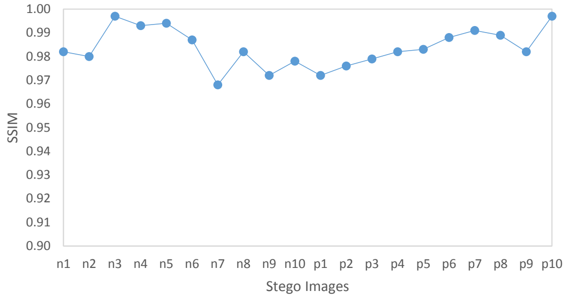

FIGURE 8. Visual comparison of stego images SSIM for patient report.

TABLE 8. Comparison of PSNR results at various image region divisions.

Region Division (%)			Threshold		PSNR				
L	M	H	t_1	t_2	Lena	Baboon	Pepper	Cameraman	Barbara
45	35	20	116	206	44.511	44.299	44.275	43.770	44.126
33	33	34	86	171	45.564	45.604	45.729	44.436	45.065
30	30	40	76	152	46.149	46.206	46.340	45.192	45.378
25	35	40	65	157	45.967	46.066	46.195	45.111	45.408
20	35	45	51	141	46.520	46.583	46.639	45.564	45.759
Only 3rd LSB			-	-	42.840	42.630	42.836	42.250	42.414

TABLE 9. Comparison of results on PSNR with the standard set of images when image dimension is 512×512 and embedding bits are 104,857.

Stego image	Muhammad et al. [49]	Rehman et al. [50]	Bailey and Curran [51]	Karim et al. [52]	Jassim [53]	Proposed (IRD)
Lena	50.011	51.045	44.117	42.954	44.931	49.827
Baboon	49.099	51.997	44.669	44.656	44.745	50.075
Peppers	39.381	49.442	35.039	31.225	34.022	50.149
Cameraman	48.023	50.981	44.585	41.559	45.213	47.884
Barbara	47.335	50.452	46.112	40.993	43.595	48.421
Average	46.769	50.783	42.904	40.277	42.501	49.271

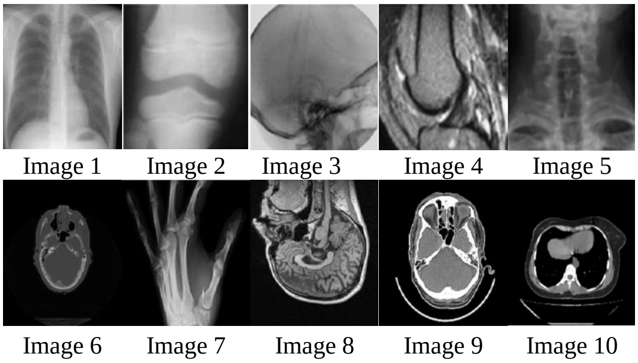

FIGURE 9. The set of randomly selected medical images of size 512×512 for comparison purpose.

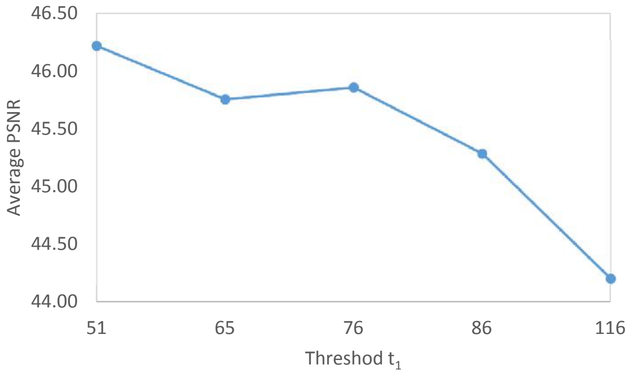

FIGURE 10. Visual presentation for various values of threshold t_1.

This section is based on the comparison of the performance of the proposed IRD method with five state-of-the-art steganography techniques. We used a standard set of widely used images for comparing the performance of steganography techniques.

The PSNR results of [49]–[53] are based on $104,857$ bits. We used a similar number of bits for the data embedding. The results of the PSNR show that the proposed IRD method significantly outperforms other four baseline methods and remain comparable with Rehman et al. [50]. Table 9 shows the comparison of PNSR based on the size of $104,857$ bits.

Since the embedding of a larger data size with a higher PSNR shows the efficiency of the stego approach, therefore, we further developed the performance of the proposed IRD method with Rehman et al. [50] by increasing the data size to $235,929$ bits. The average PSNRs are 45.870 for the proposed approach and 38.857 for Rehman et al. [50], respectively. The proposed method retains its PSNR and significantly outperforms the baseline approach, as shown in Table 10.

TABLE 10. PSNR comparison with maximum data embedding capacity.

	Embedding bits 235,929		Embedding bits 263,016
Image	Rehman et al. [50]	Proposed	Proposed
Lena	41.035	46.100	45.825
Baboon	39.728	46.276	45.959
Peppers	38.443	46.290	46.091
Cameraman	38.059	45.093	44.923
Barbara	37.022	45.592	45.202
Average	38.857	45.870	45.600

Furthermore, we evaluated the proposed method at its maximum payload capacity (i.e., $263,016$ bits). Table 10 shows the average PSNR value 45.600 at maximum payload which is significant improvement. The stego images are imperceptible because of better PSNR. The average embedding rate in terms of bits per pixel (bpp) is 1.03. The standard size of 512×512 dimension image is $262,144$ pixels.

A. COMPUTATIONAL COMPLEXITY

Let N be the number of pixels in the cover image. the embedding algorithm first performs an intensity-based image division into three regions. Therefor N number of passes required for the division mechanism. Thus, the intensity-based image division has a time complexity of $O(N)$. Iterations for each unique region take a constant time $O(1)$. The embedding loop iterates M time where M is the length of the secret data. The total asymptotic time complexity for the data embedding into a source image is $O(NM)$. In the same manner, it can be determined that the time complexity of the extraction algorithm is $O(N)$. To determine the space complexity of the proposed steganography method, the data structures whose size varies with the change of input are taken into consideration. Arrays are used to store the cover image, stego image, and secret data. The gray image with N number of pixel takes N bytes in the memory. Therefore, the space complexity of the proposed algorithm is $O(N)$.

VII. CONCLUSION AND FUTURE WORK

In this research work, we proposed a novel IRD algorithm in the image spatial domain to embed variable-sized patient secret data into MRI host images. The algorithm first segments the image into three intensity-based regions. Three least significant bits are operated in low, medium, and high-intensity regions. In the low-intensity area, the substitution of secret data bits is done on 3^{rd} LSB with the enhancement of 2^{nd} and 1^{st} LSB. In the medium intensity region two LSBs are operated, the substitution of secret data bits is done on 2^{nd} LSB, with the adjustment of 1^{st} LSB. In the high-intensity region, only 1^{st} LSB is operated and substituted with secret data bits. The algorithm is tested over a set of MRI images for both positive and negative cases. The results of the proposed IRD methods are significant in terms of imperceptibility and payload capacity. The proposed IRD method is also evaluated over a standard set of images (lena. baboon, peppers, cameraman, barbara) of 512×512 dimension. The quality and structural similarity parameters MSE, PSNR, and SSIM verify the image degradation. The MSE and PSNR values always lie within the standard range. In the future, the proposed IRD method could also be extended to other high dimensional image modalities of various parts of the body as well as to color images.

REFERENCES

[1] I. J. Kadhim, P. Premaratne, P. J. Vial, and B. Halloran, "Comprehensive survey of image steganography: Techniques, evaluations, and trends in future research," *Neurocomputing*, vol. 335, pp. 299–326, 2019.

[2] D. Artz, "Digital steganography: hiding data within data," *IEEE Internet computing*, vol. 5, no. 3, pp. 75–80, 2001.

[3] A. K. Sahu and G. Swain, "High fidelity based reversible data hiding using modified lsb matching and pixel difference," *Journal of King Saud University-Computer and Information Sciences*, 2019.

[4] H. Noda, M. Niimi, and E. Kawaguchi, "High-performance jpeg steganography using quantization index modulation in dct domain," *Pattern Recognition Letters*, vol. 27, no. 5, pp. 455–461, 2006.

[5] R. Chandramouli, "A mathematical framework for active steganalysis," *Multimedia systems*, vol. 9, no. 3, pp. 303–311, 2003.

[6] A. K. Sahu and G. Swain, "Dual stego-imaging based reversible data hiding using improved lsb matching," *Int. J. Intell. Eng. Syst.*, vol. 12, no. 5, pp. 63–73, 2019.

[7] H. Sajedi and M. Jamzad, "Bss: Boosted steganography scheme with cover image preprocessing," *Expert systems with Applications*, vol. 37, no. 12, pp. 7703–7710, 2010.

[8] W.-J. Chen, C.-C. Chang, and T. H. N. Le, "High payload steganography mechanism using hybrid edge detector," *Expert Systems with applications*, vol. 37, no. 4, pp. 3292–3301, 2010.

[9] A. Ioannidou, S. T. Halkidis, and G. Stephanides, "A novel technique for image steganography based on a high payload method and edge detection," *Expert systems with applications*, vol. 39, no. 14, pp. 11 517–11 524, 2012.

[10] D.-C. Wu and W.-H. Tsai, "A steganographic method for images by pixel-value differencing," *Pattern Recognition Letters*, vol. 24, no. 9-10, pp. 1613–1626, 2003.

[11] C.-H. Yang, C.-Y. Weng, S.-J. Wang, and H.-M. Sun, "Adaptive data hiding in edge areas of images with spatial lsb domain systems," *IEEE Transactions on Information Forensics and Security*, vol. 3, no. 3, pp. 488–497, 2008.

[12] M. Naor and A. Shamir, "Visual cryptography ii: Improving the contrast via the cover base," in *International Workshop on Security Protocols*. Springer, 1996, pp. 197–202.

[13] A. Shamir, "How to share a secret," *Communications of the ACM*, vol. 22, no. 11, pp. 612–613, 1979.

[14] C.-K. Chan and L.-M. Cheng, "Hiding data in images by simple lsb substitution," *Pattern recognition*, vol. 37, no. 3, pp. 469–474, 2004.

[15] M. Hussain, A. W. A. Wahab, Y. I. B. Idris, A. T. Ho, and K.-H. Jung, "Image steganography in spatial domain: A survey," *Signal Processing: Image Communication*, vol. 65, pp. 46–66, 2018.

[16] A. Khamrui and J. Mandal, "A genetic algorithm based steganography using discrete cosine transformation (gasdct)," *Procedia Technology*, vol. 10, pp. 105–111, 2013.

[17] S. K. Bandyopadhyay, T. U. Paul, and A. Raychoudhury, "A novel steganographic technique based on 3d-dct approach," *Computer and Information Science*, vol. 3, no. 4, p. 229, 2010.

[18] B. Kaur, A. Kaur, and J. Singh, "Steganographic approach for hiding image in dct domain," *International Journal of Advances in Engineering & Technology*, vol. 1, no. 3, p. 72, 2011.

[19] P.-Y. Chen and H.-J. Lin, "A dwt based approach for image steganography," *International Journal of Applied Science and Engineering*, vol. 4, no. 3, pp. 275–290, 2006.

[20] W.-Y. Chen, "Color image steganography scheme using dft, spiht codec, and modified differential phase-shift keying techniques," *Applied Mathematics and computation*, vol. 196, no. 1, pp. 40–54, 2008.

[21] A. K. Sahu and G. Swain, "Reversible image steganography using dual-layer lsb matching," *Sensing and Imaging*, vol. 21, no. 1, p. 1, 2020.

[22] M. Li, S. Yu, Y. Zheng, K. Ren, and W. Lou, "Scalable and secure sharing of personal health records in cloud computing using attribute-based encryption," *IEEE transactions on parallel and distributed systems*, vol. 24, no. 1, pp. 131–143, 2012.

[23] H. Sajedi, "Applications of data hiding techniques in medical and healthcare systems: a survey," *Network Modeling Analysis in Health Informatics and Bioinformatics*, vol. 7, no. 1, p. 6, 2018.

[24] S. Arunkumar, V. Subramaniyaswamy, V. Vijayakumar, N. Chilamkurti, and R. Logesh, "Svd-based robust image steganographic scheme using riwt and dct for secure transmission of medical images," *Measurement*, vol. 139, pp. 426–437, 2019.

[25] R. J. Anderson and F. A. Petitcolas, "On the limits of steganography," *IEEE Journal on selected areas in communications*, vol. 16, no. 4, pp. 474–481, 1998.

[26] A. Cheddad, J. Condell, K. Curran, and P. Mc Kevitt, "Digital image steganography: Survey and analysis of current methods," *Signal processing*, vol. 90, no. 3, pp. 727–752, 2010.

[27] X. Liao, J. Yin, S. Guo, X. Li, and A. K. Sangaiah, "Medical jpeg image steganography based on preserving inter-block dependencies," *Computers & Electrical Engineering*, vol. 67, pp. 320–329, 2018.

[28] M. Sajjad, K. Muhammad, S. W. Baik, S. Rho, Z. Jan, S.-S. Yeo, and I. Mehmood, "Mobile-cloud assisted framework for selective encryption of medical images with steganography for resource-constrained devices," *Multimedia Tools and Applications*, vol. 76, no. 3, pp. 3519–3536, 2017.

[29] N. Alsaidi, M. Alshareef, A. Alsulami, M. Alsafri, and A. Aljahdali, "Digital steganography in computer forensics," *International Journal of Computer Science and Information Security (IJCSIS)*, vol. 18, no. 5, 2020.

[30] M. Elhoseny, G. Ramírez-González, O. M. Abu-Elnasr, S. A. Shawkat, N. Arunkumar, and A. Farouk, "Secure medical data transmission model for iot-based healthcare systems," *IEEE Access*, vol. 6, pp. 20 596–20 608, 2018.

[31] N. K. Mansor, S. M. H. Asraf, and S. Z. S. Idrus, "Steganographic on pixel value differencing in iris biometric," in *Journal of Physics: Conference Series*, vol. 1529, no. 3. IOP Publishing, 2020, p. 032078.

[32] A. Shehab, M. Elhoseny, K. Muhammad, A. K. Sangaiah, P. Yang, H. Huang, and G. Hou, "Secure and robust fragile watermarking scheme for medical images," *IEEE Access*, vol. 6, pp. 10 269–10 278, 2018.

[33] H.-Y. Lee, "Adaptive reversible watermarking for authentication and privacy protection of medical records," *Multimedia Tools and Applications*, pp. 1–18, 2019.

[34] J. A. Kaw, N. A. Loan, S. A. Parah, K. Muhammad, J. A. Sheikh, and G. M. Bhat, "A reversible and secure patient information hiding system for iot driven e-health," *International Journal of Information Management*, vol. 45, pp. 262–275, 2019.

[35] S. A. Parah, F. Ahad, J. A. Sheikh, N. A. Loan, and G. M. Bhat, "A new reversible and high capacity data hiding technique for e-healthcare applications," *Multimedia Tools and Applications*, vol. 76, no. 3, pp. 3943–3975, 2017.

[36] R. Karakış, İ. Güler, I. Capraz, and E. Bilir, "A novel fuzzy logic-based image steganography method to ensure medical data security," *Computers in biology and medicine*, vol. 67, pp. 172–183, 2015.

[37] K. Rabah, "Steganography-the art of hiding data," *Information Technology Journal*, vol. 3, no. 3, pp. 245–269, 2004.

[38] A. K. Sahu and G. Swain, "An optimal information hiding approach based on pixel value differencing and modulus function," *Wireless Personal Communications*, vol. 108, no. 1, pp. 159–174, 2019.

[39] A. K. Sahu and G. Swain, "A novel n-rightmost bit replacement image steganography technique," *3D Research*, vol. 10, no. 1, p. 2, 2019.

[40] A. K. Sahu and G. Swain, "Pixel overlapping image steganography using pvd and modulus function," *3D Research*, vol. 9, no. 3, p. 40, 2018.

[41] A. K. Sahu, G. Swain, and E. S. Babu, "Digital image steganography using bit flipping," *Cybernetics and Information Technologies*, vol. 18, no. 1, pp. 69–80, 2018.

[42] R. Wazirali and Z. Chachzo, "Hyper edge detection with clustering for data hiding," *Journal of Information Hiding and Multimedia Signal Processing (JIHMSP)*, 2015.

[43] Z. Wang, Z. Qian, X. Zhang, M. Yang, and D. Ye, "On improving distortion functions for jpeg steganography," *IEEE Access*, vol. 6, pp. 74 917–74 930, 2018.

[44] F. Li, K. Wu, X. Zhang, J. Yu, J. Lei, and M. Wen, "Robust batch steganography in social networks with non-uniform payload and data decomposition," *IEEE Access*, vol. 6, pp. 29 912–29 925, 2018.

[45] J. Tao, S. Li, X. Zhang, and Z. Wang, "Towards robust image steganography," *IEEE Transactions on Circuits and Systems for Video Technology*, vol. 29, no. 2, pp. 594–600, 2018.

[46] S. Li and X. Zhang, "Toward construction-based data hiding: from secrets to fingerprint images," *IEEE Transactions on Image Processing*, vol. 28, no. 3, pp. 1482–1497, 2018.

[47] Z. Wang, A. C. Bovik, H. R. Sheikh, and E. P. Simoncelli, "Image quality assessment: from error visibility to structural similarity," *IEEE transactions on image processing*, vol. 13, no. 4, pp. 600–612, 2004.

[48] N. A. Loan, S. A. Parah, J. A. Sheikh, J. A. Akhoon, and G. M. Bhat, "Hiding electronic patient record (epr) in medical images: A high capacity and computationally efficient technique for e-healthcare applications," *Journal of biomedical informatics*, vol. 73, pp. 125–136, 2017.

[49] K. Muhammad, J. Ahmad, H. Farman, Z. Jan, M. Sajjad, S. W. Baik *et al.*, "A secure method for color image steganography using gray-level modification and multi-level encryption." *TIIS*, vol. 9, no. 5, pp. 1938–1962, 2015.

[50] A. Rehman, T. Saba, T. Mahmood, Z. Mehmood, M. Shah, and A. Anjum, "Data hiding technique in steganography for information security using number theory," *Journal of Information Science*, vol. 45, no. 6, pp. 767–778, 2019.

[51] K. Bailey and K. Curran, "An evaluation of image based steganography methods," *Multimedia Tools and Applications*, vol. 30, no. 1, pp. 55–88, 2006.

[52] S. M. Karim, M. S. Rahman, and M. I. Hossain, "A new approach for lsb based image steganography using secret key," in *14th International Conference on Computer and Information Technology (ICCIT 2011)*. IEEE, 2011, pp. 286–291.

[53] F. A. Jassim, "A novel steganography algorithm for hiding text in image using five modulus method," *arXiv preprint arXiv:1307.0642*, 2013.

GHAZANFAR FAROOQ SIDDIQUI is an Assistant Professor at Department of Computer Science at Quaid-i-Azam University, Islamabad. Earlier, he was a research Scholar in Department of Computer Science, Vrije Universiteit Amsterdam, The Netherlands. He received his Ph.D from Vrije Universiteit Amsterdam in 2010. The Ph.D scholarship was funded by Higher Education Commission, Pakistan.

He is a reviewer of a number of peer reviewed conferences and Journals. He also published numerous research papers in reputed conferences and Journals. He is a member of Federal Public Service Commission and Khyber Pakhtunkhwa Public Service Commission. He is also serving as an evaluator for scientific projects of Directorate of Science and Technology (DoST) - Khyber Pakhtunkhwa. Furthermore, He is a member of Board of Studies of Quaid-i-Azam University, Islamabad and National Textile University, Faisalabad.

MUHAMMAD ZAFAR IQBAL is a Faculty Member of Computer Science, The Islamia University of Bahawalpur. Currently, he is a Ph.D. Scholar with the Department of Computer Science, Quaid-i-Azam University, Islamabad. His research interest includes Image Analysis and Processing, Computer Vision, Artificial Intelligence, and Machine learning.

KHALID SALEEM received the M.Sc. degree from Quaid-i-Azam University, Pakistan, in 1994, and the M.Phil. and Ph.D. degrees from the University of Montpellier 2, France, in 2005 and 2008, respectively, all in computer science. He was with the software industry from last 20 years. He is currently an Assistant Professor with Quaid-i-Azam University. He has authored more than 30 research papers and various scientific reports and book chapters. His research interests include data mining, schema matching and integration, database systems, bioinformatics, distributed systems, and data warehousing.

ZAFAR SAEED received a Ph.D. and M.Phil degrees from the Department of Computer Science, Quaid-i-Azam University, Islamabad, Pakistan, in 2010 and 2020. He was a research fellow with the University of Technology Sydney, Australia, during 2017-2018. He has been working on social media network and content analysis and published several articles in high impact factor journals. His research interests include temporal data streams, social media analytics, and machine learning.

ADEEL AHMED received the M.Phil. degree in computer science from Quaid-i-Azam University, Islamabad, Pakistan, in 2011, where he is currently a Ph.D. Scholar with the Department of Computer Science. He was granted a travel award in HUGO 15th Human Genome Meeting, Dubai, United Arab Emirates, in 2011. He is currently a Faculty Member of Computer Science, National University of Modern Languages, Islamabad. He has authored more than ten research papers. His research interests include large scale complex schema matching and integration using machine learning, recommendation systems, social network analysis, and bioinformatics with a focus on simulation techniques.

IBRAHIM A. HAMEED is a Professor at the Department of ICT and Natural Sciences, Faculty of Information Technology and Electrical Engineering, Norwegian University of Science, and Technology (NTNU), Norway. Hameed is Deputy Head of research and innovation within the same department. He is also program coordinator of the department's international master program in simulation and visualization. Among others, Hameed is an IEEE senior member and elected chair of the IEEE Computational Intelligence Society (CIS) Norway section. Hameed has a Ph.D. degree in Industrial Systems and Information Engineering from Korea University, Seoul, South Korea and a PhD degree in Mechanical Engineering from Aarhus University, Aarhus, Denmark. He is author of more than 120 journal and conference articles. His current research interest includes Artificial Intelligence, Machine Learning, Optimization, and Robotics.

MUHAMMAD FAHAD KHAN is currently an Assistant Professor with Foundation University and a Ph.D. Scholar with the Department of Computer Science, Quaid-i-Azam University, Islamabad. He has authored more than 30 research papers. His research interests include steganography, cryptography, and multimedia communication.

• • •